Inorganic Chemistry

Article

pubs.acs.org/IC

Homoleptic Iron(II) Complexes with the Ionogenic Ligand 6,6′-Bis(1*H*-tetrazol-5-yl)-2,2′-bipyridine: Spin Crossover Behavior in a Singular 2D Spin Crossover Coordination Polymer

Maksym Seredyuk,*[,†,‡] Lucía Piñeiro-López,[†] M. Carmen Muñoz,[§] Francisco J. Martínez-Casado,[∥] Gábor Molnár,[⊥] José Alberto Rodriguez-Velamazán,[#] Azzedine Bousseksou,[⊥] and José Antonio Real*[,†]

[†]Instituto de Ciencia Molecular (ICMol), Universidad de Valencia, 46980 Paterna, Valencia, Spain

[‡]Department of Physical Chemistry, National Taras Shevchenko University, Volodymyrska Str. 64, Kiev 01601, Ukraine

[§]Departamento de Física Aplicada, Universitat Politècnica de València, 46022 Valencia, Valencia, Spain

[∥]MAX IV Laboratory, Lund University, Ole Römers väg 1., 223 63 Lund, Sweden

[⊥]LCC, CNRS & Université de Toulouse (UPS, INP), 205 route de Narbonne, F-31077 Toulouse, France

[#]Instituto de Ciencia de Materiales de Aragón (ICMA), CSIC and Universidad de Zaragoza and Institut Laue-Langevin, 38042 Grenoble Cedex 9, France

Supporting Information

ABSTRACT: Deprotonation of the ionogenic tetradentate ligand 6,6′-bis(1*H*-tetrazol-5-yl)-2,2′-bipyridine [H_2bipy(ttr)$_2$] in the presence of Fe^{II} in solution has afforded an anionic mononuclear complex and a neutral two-dimensional coordination polymer formulated as, respectively, NEt_3H{Fe[bipy(ttr)$_2$][Hbipy(ttr)$_2$]}·3MeOH (**1**) and {Fe[bipy(ttr)$_2$]}$_n$ (**2**). The anions [Hbipy(ttr)$_2$]$^-$ and [bipy(ttr)$_2$]$^{2-}$ embrace the Fe^{II} centers defining discrete molecular units **1** with the Fe^{II} ion lying in a distorted bisdisphenoid dodecahedron, a rare example of octacoordination in the coordination environment of this cation. The magnetic behavior of **1** shows that the Fe^{II} is high-spin, and its Mössbauer spectrum is characterized by a relatively large average quadrupole splitting, ΔE_Q = 3.42 mm s^{-1}. Compound **2** defines a strongly distorted octahedral environment for Fe^{II} in which one [bipy(ttr)$_2$]$^-$ anion coordinates the equatorial positions of the Fe^{II} center, while the axial positions are occupied by peripheral *N*-tetrazole atoms of two adjacent {Fe[bipy(ttr)$_2$]}^{0} moieties thereby generating an infinite double-layer sheet. Compound **2** undergoes an almost complete spin crossover transition between the high-spin and low-spin states centered at about 221 K characterized by an average variation of enthalpy and entropy ΔH^{av} = 8.27 kJ mol^{-1}, ΔS^{av} = 37.5 J K^{-1} mol^{-1}, obtained from calorimetric DSC measurements. Photomagnetic measurements of **2** at 10 K show an almost complete light-induced spin state trapping (LIESST) effect which denotes occurrence of antiferromagnetic coupling between the excited high-spin species and T_{LIESST} = 52 K. The crystal structure of **2** has been investigated in detail at various temperatures and discussed.

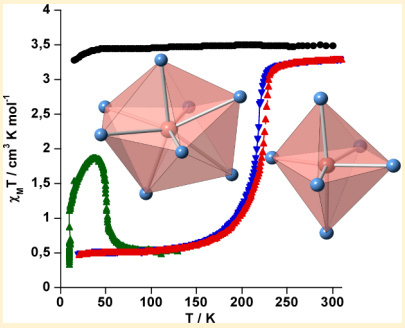

INTRODUCTION

Fe^{II} spin crossover (SCO) complexes reversibly change between the S = 2 high-spin (HS) state and the S = 0 low-spin state (LS) with concomitant changes in their physical properties (magnetic, optical, dielectric) and structure.[1] This SCO behavior, induced by external stimuli such as temperature and/or pressure variations, light irradiation, or analytes, has stimulated much interest in the realm of switchable molecular materials since it has been claimed that Fe^{II} SCO compounds could potentially be used for the fabrication of devices for information storage, i.e., memories and sensors working at reasonable high temperatures.[2] Thus, the search for new Fe^{II} SCO complexes and their processing is a topic of current concern in chemistry and science of materials.[3]

Most Fe^{II} SCO compounds exhibit a pseudo-octahedral [FeN_6] coordination core. For an important number of them the nitrogen atoms belong to neutral heterocyclic organic ligands, thus resulting in discrete cationic complexes whose charge is counterbalanced by noncoordinating anions (ClO_4^-, BF_4^-, PF_6^-, etc.).[4] However, the ligand field strength can be appropriately adjusted and the charge balanced using ancillary pseudohalide anions (NCX^-, X = S, Se, BH_3, NCN) or polynitrile anions in combination with di- and tetradentate ligands bearing imino or imino-amino donor groups.[4−7] The resulting complexes constitute a relevant vast family of neutral SCO compounds ranging from discrete mononuclear and dinuclear to one- and two-dimensional coordination polymers. Neutral Fe^{II} SCO coordination polymers made up of self-assembly of di-, tetra-, hexa-, or octa-cyano metalate complexes, Fe^{II}, and imine ligands constitute a more recent series of

Received: May 4, 2015
Published: July 14, 2015

DOI: 10.1021/acs.inorgchem.5b01001
Inorg. Chem. 2015, 54, 7424−7432

important SCO compounds with new interesting phenomenologies.[7]

In contrast to the above-mentioned examples, the number of neutral Fe^{II} SCO complexes derived from heterocyclic organic ligands bearing ionogenic groups is relatively small. As far as we know, $Fe[HB(pz)_3]_2$ where $[HB(pz)_3]^-$ = (hydrido)tris(1*H*-pyrazol-1-yl)borate represents the first example of this class of Fe^{II} SCO complex.[8] Latter on, thermal- and light-induced SCO was investigated for the heteroleptic complexes $\{Fe[H_2B(pz)_2]_2L\}$ where $[H_2B(pz)_2]^-$ is the dihydrobispyrazolylborate anion and L = 1,10-phenanthroline or 2,2′-bipyridine.[9] Both complexes have constituted new platforms to investigate the SCO phenomenon at the nanometric scale in thin films and even at the scale of a single molecule. For example, it was shown that both derivatives can be processed as thin films, prepared by vacuum deposition, practically preserving the original magnetic and photomagnetic behavior of the bulk material.[10] Reversible and selective spin state switching of single molecules of the phen derivative was also observed in these films.[11] The search for new sublimable complexes with interesting SCO properties has motivated the synthesis of the ionogenic three-dentate ligand (2-(1*H*-pyrazol-1-yl)-6-(1*H*-tetrazol-5-yl)pyridine) (HL1) and the corresponding neutral complex $[Fe(L)_2]$ which displays cooperative SCO at room temperature (Chart 1).[12] More recently, the magnetic and photomagnetic properties of the compound $[Fe(mphenbi)_2]\cdot 2CHCl_3$ derived from the ionogenic ligand Hmphenbi (2-(1*H*-benzoimidazol-2-yl)-9-methyl-1,10-phenanthroline) have been reported.[13]

Chart 1. Relevant Ionogenic Ligands

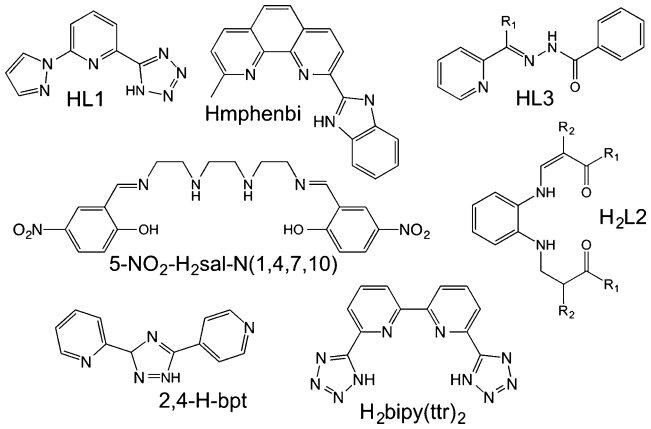

All the aforementioned neutral SCO complexes with ionogenic organic ligands feature the $[FeN_6]$ chromophore. However, a series of neutral Fe^{II} SCO complexes with less common $[N_4O_2]$ chromophore have also been reported. As far as we know, the first known example is the mononuclear Fe^{II} compound $[Fe(5\text{-}NO_2\text{-}sal\text{-}N(1,4,7,10)]$ which manifests simultaneously strong cooperative two-step SCO and crystallographic phase transition. The hexadentate ligand 5-NO_2-sal-N(1,4,7,10) is a typical Schiff base resulting from condensation of 5-nitrosalicylaldehyde with tetraazadecane in a 2:1 ratio.[14] A more stable series of neutral Fe^{II} SCO complexes formulated $[Fe(L2)(L)_x]$ have been obtained from combination of the equatorial planar tetradentate Jäger's $[N_2O_2]$ Schiff-like bases (H2L2), Fe^{II}, and the ancillary axial pyridine-like monodentate (x = 2) or bis-monodentate (x = 1) ligands.[15] More recently, a new type of homoleptic $[Fe(L3)_2]$ SCO complexes with $[N_4O_2]$ chromophore has been reported. They are constituted of tridentate HL3 ligands with $[N_2O]$ chromophore derived from the *N*′-((pyridin-2-yl)methylene)benzohydrazide.[16]

Except for a series of 1D SCO complexes derived from Jäger-type ligand, all neutral SCO complexes obtained from the ionogenic heterocyclic ligands mentioned so far afford discrete (0D) compounds. Only two examples of 2D coordination polymers undergoing SCO behavior have been reported. The compound $[Fe_2(2,2'\text{-bipyridine})(imidazolate)_4]$ forms extended 2D double-layer sheets of alternating tetrahedral and octahedral Fe^{II} centers; each Fe^{II} is bridged to four others by single imidazolate ligands. Chelating 2,2′-bipy ligands occupy the remaining coordination sites of the octahedral centers. This compound shows two crystallographic phase transitions accompanied by an abrupt SCO centered at 135 K.[17] There is the SCO system $[Fe(2,4\text{-bpt})_2]\cdot nH_2O$ where 2,4-bpt$^-$ is the deprotonated form of 2,4-H-bpt = 3-(2-pyridyl)-5-(4-pyridyl)-1,2,4-triazole). Here, 2,4-bpt$^-$ acts simultaneously as a chelate bidentate ligand (through 2-pyridyl-1,2,4-triazole moiety) and as monodentate ligand (through 4-pyridyl moiety). In the anhydrous derivative (n = 0) the monodentate moiety coordinates the Fe^{II} centers in trans configuration; however, for n = 4 the coordination is cis. The latter form undergoes quite incomplete and gradual SCO. However, thermal-driven supramolecular isomerism and complete dehydration in the solid state transform the cis conformation to the trans conformation, which undergoes a complete and more cooperative SCO behavior centered at ca. 275 K.[18]

As a new step in this direction, here we report two unprecedented Fe^{II} neutral complexes, the mononuclear $NEt_3H\{Fe[bipy(ttr)_2][Hbipy(ttr)_2]\}\cdot 3MeOH$ (**1**) and the two-dimensional coordination polymer $\{Fe[bipy(ttr)]_2\}_n$ (**2**) derived, respectively, from partial and complete deprotonation of the tetradentate ionogenic ligand $[H_2bipy(ttr)_2]$ (6,6′-bis(1*H*-tetrazol-5-yl)-2,2′-bipyridine). We report the synthesis, the structural analysis, the Mössbauer spectra, and the magnetic properties of **1** and **2** as well as the photomagnetic and differential scanning calorimetry (DSC) measurements of **2**.

RESULTS AND DISCUSSION

Synthesis. We have synthesized the tetrazole-based ligands $[H_2bipy(ttr)_2]$ following the already described thermal cycloaddition reaction of sodium azide with the 2,2′-bipyridine-6,6′-dicarbonitrile in anhydrous DMF in the presence of NH_4Cl.[19] The crystals of mononuclear complex **1** were obtained by reaction of 2 equiv of deprotonated ligand with Fe^{II} salt in methanol. The reaction of ligand with Fe^{II} salt under slow diffusion resulted in autodeprotonation of the ligand and formation of two-dimensional coordination polymer **2**.

Structure. *Structure of 1.* Compound **1** displays the monoclinic $P2_1/c$ space group at 120 K. A selection of the crystal data and bond lengths and angles of the coordination core $[FeN_8]$ is gathered in Tables 1 and 2, respectively. Figure 1a shows an ORTEP representation of the asymmetric unit together with the atom numbering. The Fe^{II} is surrounded by two tetradentate $[bipy(ttr)_2]^-$ anionic ligands disposed in *mer* conformation through N(1), N(2), N(3), N(4) (ligand 1) and N(11), N(12), N(13), N(14) (ligand 2) defining a distorted bisdisphenoid dodecahedron with approximate D_{2d} symmetry, a rare coordination for Fe^{II} (see Figure 1b). The Fe−N bond lengths of the Fe−N(bipy) moieties, found in the range 2.38−2.42 Å, are much longer than those of the Fe−N(tetrazole): Fe−N(1) = 2.261(3) Å, Fe−N(4) = 2.310(3) Å, Fe−N(11) =

DOI: 10.1021/acs.inorgchem.5b01001
Inorg. Chem. 2015, 54, 7424−7432

Table 1. Crystal Data for Compounds 1 and 2[a]

	1	2	
empirical formula	$C_{33}H_{41}N_{21}O_3Fe$	$C_{12}H_6N_{10}Fe$	
M_r	835.72	346.12	
cryst syst	monoclinic	orthorhombic	
space group	$P2_1/c$	*Pbca*	
T (K)	120(1)	100(2)	298(2)
a (Å)	17.3066(5)	13.861(3)	13.741(3)
b (Å)	11.3516(3)	8.245(2)	9.346(2)
c (Å)	21.8806(12)	20.792(4)	20.294(4)
β (deg)	116.250(3)		
V (Å^3)	3855.3(3)	2376.2(8)	2606.2(9)
Z	4	8	
D_c (mg cm^{-3})	1.440	1.935	1.764
F(000)	1744	1392	
μ (Mo Kα) (mm^{-1})	0.457	1.769	1.613
cryst size (mm^3)	0.04 × 0.10 × 0.10	0.05 × 0.06 × 0.08	
no. total reflns	9892	2952	2662
no. reflns [$I > 2\sigma(I)$]	7166	2736	2435
R [$I > 2\sigma(I)$]	0.0656	0.0400	0.0348
R [all data]	0.0912	0.0449	0.0376
S	0.950	1.168	0.864

[a] $R_1 = \sum(|F_o| - |F_c|)/\sum|F_o|$; wR = $[\sum[w(F_o^2 - F_c^2)^2]/\sum[w(F_o^2)^2]]^{1/2}$; $w = 1/[\sigma^2(F_o^2) + (mP)^2 + nP]$ where $P = (F_o^2 + 2F_c^2)/3$; m = 0.1129 (**1** (120 K)), 0.0558 (**2** (100 K)), 0.0966 (**2** (298 K)); n = 5.6335 (**1** (120 K)), 6.0456 (**2** (100 K)), 4.4896 (**2** (298 K)).

Table 2. Selected Bond Lengths [Å] for 1 and 2

		2	
	1 at 120 K	100 K	298 K
Fe(1)−N(1)	2.260(2)	1.923(2)	2.161(2)
Fe(1)−N(2)	2.390(2)	1.916(2)	2.158(2)
Fe(1)−N(3)	2.416(2)	2.063(2)	2.125(2)
Fe(1)−N(4)	2.310(2)		
Fe(1)−N(5)		2.002(2)	2.202(2)
Fe(1)−N(7)		2.040(2)	2.135(2)
Fe(1)−N(10)		2.008(2)	2.215(2)
Fe(1)−N(11)	2.241(3)		
Fe(1)−N(12)	2.385(2)		
Fe(1)−N(13)	2.379(2)		
Fe(1)−N(14)	2.240(3)		

2.240(3) Å, Fe−N(14) = 2.240(3) Å. The significantly longer Fe−N(4) bond length suggests that the corresponding tetrazolate moiety remains protonated. Indeed, the hydrogen atom H1 attached to N10 was located unambiguously by Fourier difference synthesis. In general, the bond lengths are close to those found for the complexes $[Fe(L_{N4}H_2)](BPh_4)_2 \cdot Et_2O$ ($L_{N4}H_2$ is the macrocyclic ligand 2,11-diaza[3.3](2,6)-pyridinophane)[20] and [Fe(L_{N4})2](BF_4)2 (L_{N4} results from the condensation of 1,2-phenylenediamine with 2 equiv of 1-methyl-2-imidazole carboxaldehyde)[21] whose coordination environments correspond to a distorted dodecahedron and a distorted square antiprism, respectively. To the best of our knowledge, only four additional Fe^{II} complexes with coordination number 8 have been crystallographically described in addition to the two latter complexes: Fe(1,8-naphtypyridine)$_3$(ClO_4)$_2$;[22] the solid solution $[FeL]_{0.31}[FeL']_{0.69}[PF_6]_2 \cdot 0.5(CH_3)_2CO \cdot 0.5C_2H_5OH$, where L is the 1,4,7,10-tetraazacyclododecane ligand with a pyrazol-1-ylmethyl moiety attached to each amine group and L′ is the same macrocycle with only

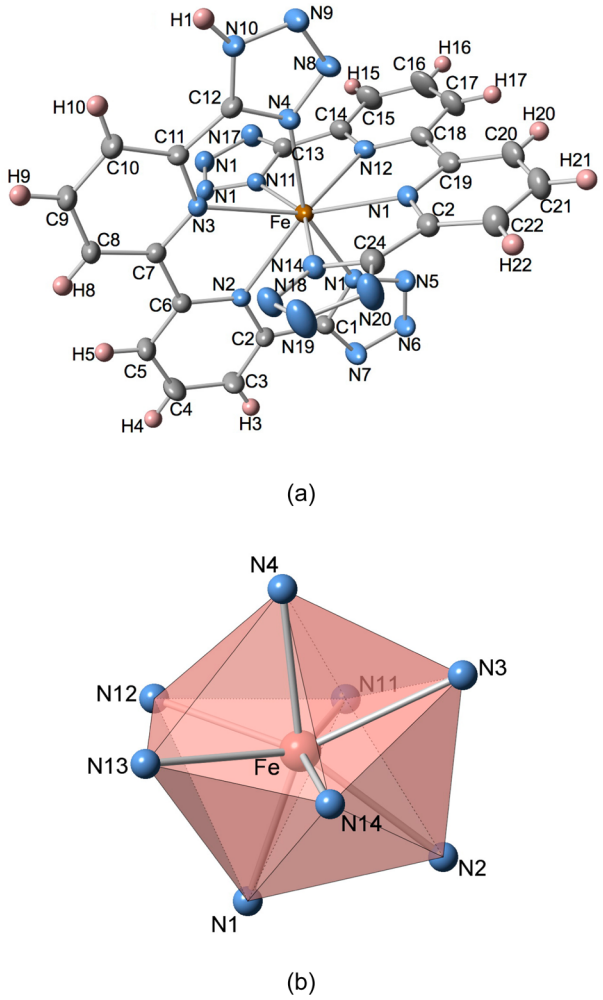

Figure 1. (a) ORTEP representation of the neutral molecule **1**. (b) Coordination polyhedron showing the distorted bisdisphenoid dodecahedron. Thermal ellipsoids are represented at 50% probability level. Color code: Fe, light red; N, blue; C, gray; H, pink.

three substituted amine groups;[23] $[Fe(TPA)_2](BPh_4)_2$, where TPA is the tris(2-pyridylmethyl)amine;[24] and [Fe(cyclen-py_4](ClO_4)$_2$·H_2O, where cyclen-py_4 results from functionalization the four amine groups of the tetraazacyclododecane macrocyclic with 2-methylpyridine moiety.[25] In all cases the Fe−N bond lengths are typical of the Fe^{II} ion in the HS state. The crystal packing of **1** can be described as an infinite stack of layers parallel to the $a-b$ plane. The layers are made up of neutral complexes which interact with each other through strong $\pi-\pi$ interactions, see Table 3 and Figure 2. The layers stack along the c axis and are separated by the protonated triethylamonium cation, which balances the charge of the complex, and methanol molecules. The N−H moiety of the triethylamonium defines a hydrogen bond with the oxygen atom of a methanol molecule (d[N(21)···O(2) = 3.066(8) Å; (x, $-y - {}^1/_2$, $z - {}^1/_2$)]). Furthermore, two methanol molecules interact with each other through strong hydrogen bonds (d[O(3)···O(2)] = 2.613(7) Å).

Structure of 2. The crystal structure of **2** has been solved at 298 and 100 K. At both temperatures the crystal displays the orthorhombic *Pbca* space group. A selection of crystal data and bond lengths and angles of the coordination core [FeN_6] is gathered in Tables 1 and 2, respectively. In addition, the

DOI: 10.1021/acs.inorgchem.5b01001
Inorg. Chem. 2015, 54, 7424−7432

Table 3. Relevant Interlayer C···C Short Contacts [Å] for 2[a]

	100 K	298 K
C(1)···C(1)	3.591(4)i	3.674(3)i
C(1)···C(2)	3.448(4)i	3.765(3)i
C(1)···C(6)	3.722(3)i	3.591(3)i
C(2)···C(4)	3.399(4)ii	3.882(4)ii
C(2)···C(6)	3.225(3)i	3.341(3)i
C(2)···C(7)	3.430(3)i	3.532(4)i
C(3)···C(3)	3.497(3)ii	3.928(4)ii
C(3)···C(4)	3.226(3)ii	3.364(4)ii
C(3)···C(5)	3.421(3)ii	3.607(4)ii
C(3)···C(6)	3.459(4)i	3.746(4)i
C(3)···C(7)	3.253(3)i	3.563(4)i
C(3)···C(8)	3.422(3)i	3.491(4)i
C(3)···C(9)	3.758(3)i	3.616(4)i
C(4)···C(4)	3.532(3)ii	3.322(4)ii
C(4)···C(7)	3.467(4)i	3.707(4)i
C(4)···C(8)	3.503(3)i	3.492(4)i

[a]Symmetry code: i (2 − x, −y, 1 − z); ii (2 − x, 1 − y, 1 − z).

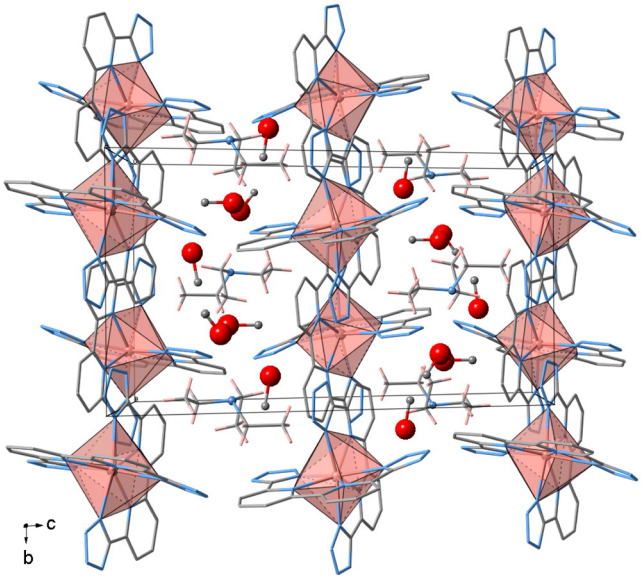

Figure 2. Fragment of the crystal packing of 1 seen along [100] direction showing the complex units and the trimethyl amine and the methanol inclusions.

evolution of the crystal structure has also been checked at different temperatures in the cooling (270, 250, 225, 212, 200, and 150 K) and heating (175, 200, 212, 225, 250, 270 K) modes.

In contrast to 1, each Fe^{II} center in 2 is coordinated only to one complete $[bipy(ttr)_2]_2^-$ ligand which occupies the four equatorial positions of a strongly distorted elongated octahedron through the N(1), N(2) atoms of the 2,2′-bipyridine moiety and N(3) and N(7) of the two tetrazole moieties. The axial positions are occupied by the peripheral atoms N(5) and N(10) of the tetrazolate moieties belonging to two equivalent $\{Fe[bipy(ttr)_2]\}$ building blocks. Figure 3 shows the resulting asymmetric unit together with the atom numbering. The average equatorial and axial Fe−N bond lengths are, respectively, 2.1446(19) and 2.2081(19) Å at 298 K and 1.9855(19) and 2.0050(19) Å at 100 K. The average bond length of the [Fe−N6] site at 298 K and at 100 K is 2.1658(19) and 1.9920(19) Å, values consistent with the HS and LS state

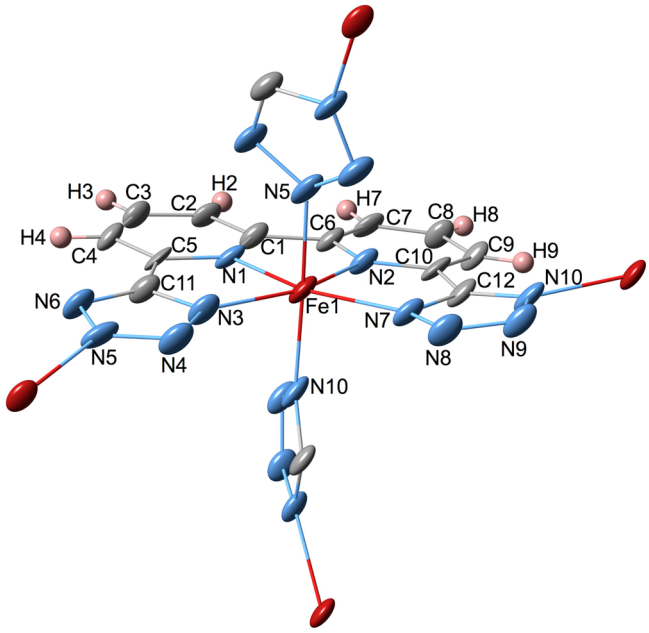

Figure 3. ORTEP representation of a representative fragment of 2. Thermal ellipsoids are represented at 50% probability level. Color code: Fe, light red; N, blue; C, gray; H, pink.

of the Fe^{II} ion, respectively. The difference between the two average values, ΔR = 0.174(2) Å, is slightly shorter than expected for a complete SCO which is close to 0.2 Å. Then, on this basis a residual fraction of ca. 13% of HS Fe^{II} centers remain at 100 K. The change of Fe−N bond lengths upon SCO is rather inhomogeneous. Thus, the average bond lengths involving the bipy moiety (Fe−N(1) and Fe−N(2)) show the remarkable change of 0.2399 Å, while that of the tetrazole moieties of the same $[bipy(ttr)_2]^{2-}$ ligand (Fe−N(3) and Fe−N(7)) change only 0.0783 Å. However, the average bond length change of the axially coordinated tetrazole groups belonging to the adjacent $\{Fe[bipy(ttr)_2]\}$ units (Fe−N(5) and Fe−N(10)) is 0.2031 Å.

The strong distortion of the coordination site is more obvious when considering the N−Fe−N angles, particularly those lying in the equatorial plane due to the rigid structure of the $[bipy(ttr)_2]^{2-}$ ligand. Thus, at 298 K, the angles N(1)−Fe−N(2), N(1)−Fe−N(3), and N(2)−Fe−N(7) are far from what is expected for a regular octahedron (90°) 72.30(7)°, 75.16(7)°, and 74.79(7)°, respectively. These angles increase by ca. 7.95(8)° (ca. 10% change), 4.34(8)°, and 4.17(8)° at 100 K. However, the most remarkable distortion is observed for the angle N(3)−Fe−N(7) which is 47.7° and 31.3° larger than 90° at 298 and 100 K, respectively. In contrast to the aforementioned small variation of the Fe−N(3) and Fe−N(7) bond lengths upon SCO, it is obvious that the N(3)−Fe−N(7) angle defined by them expresses much more markedly the spin state change since this angle changes by 16.4° (ca. 13%). The sum of the deviations from 90° of the 12 N−Fe−N angles of the $[FeN_6]$ octahedron, $\sum = (|\theta - 90|)$, is 122° (298 K) and 81.4° (100 K).

The tetrazole moieties of each $\{Fe[bipy(ttr)_2]\}$ unit link adjacent units, thereby generating undulated double-layer sheets, which spread in the $a-b$ plane and stack along the c direction (Figure 4). The aromatic rings of the bipyridine moieties of two consecutive layers interdigitate defining $\pi-\pi$ strong short contacts both at 100 and 298 K. The short

DOI: 10.1021/acs.inorgchem.5b01001
Inorg. Chem. 2015, 54, 7424−7432

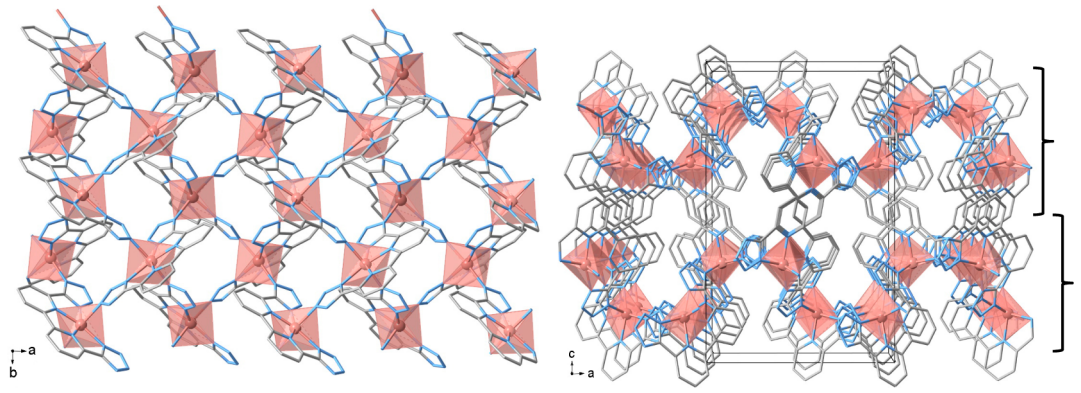

Figure 4. Crystal packing of **2**: fragment of a layer viewed down [001] direction (left) and two consecutive double-layer sheets stacked along [001] viewed down [010] direction (right).

contacts smaller than the sum of the van der Waals radii of C···C (ca. 3.59 Å) are gathered in Table 3.

The variation of the unit cell parameter c reflects the presence of strong C···C contacts at low and high temperatures. Indeed a significant increase of c takes place during the SCO together with a smaller increase of a. These are compensated by a large decrease of the b parameter (Figure 5). The thermal dependence of the unit cell volume (V) and $\chi_M T$ versus T curve (χ_M is the molar magnetic susceptibility and T is temperature) match reasonably well (Figure 5). However, it deserves to be stressed that the thermal variation of V does not show any hysteretic behavior (vide infra). This fact supports the idea that the SCO behavior of **2** is a subject of kinetic effects. The variation of the unit cell volume ΔV per Fe^{II} atom ($Z = 8$) is ca. 28.8 $Å^3$, a typical value that accounts for thermal contraction/expansion and the volume change associated with the SCO change.

It is interesting to stress some formal similitudes between **2** and compound $[Fe_2(2,2'\text{-bipyridine})(imidazolate)_4]$. In this compound one Fe^{II} is surrounded by a 2,2′-bipyridine ligand and four imidazolate bridging ligands defining an octahedral site. However, each imidazolate ligand is shared with a tetrahedral Fe^{II} site defining $[Fe^{II}(imidazolate)_4]^{2-}$ thereby originating the double-layer sheets.[17]

Magnetic Properties. The magnetic properties of compounds **1** and **2** are shown in Figure 6 in the form of the product $\chi_M T$ versus T (χ_M is the molar magnetic susceptibility, and T is temperature). At 300 K, the $\chi_M T$ value is 3.47 and 3.28 $cm^3\ K\ mol^{-1}$ for **1** and **2**, respectively. These values are typical for an $S = 2$ ground state with noticeable orbital contribution as usually observed for the Fe^{II} ion in the HS state. $\chi_M T$ remains practically constant down to 45 K for **1** and slightly decreases at lower temperatures most probably due to zero-field splitting of the $S = 2$ ground state. In contrast, $\chi_M T$ of **2** decreases rapidly in the interval 215−210 K to attain a value of 1.5 $cm^3\ K\ mol^{-1}$ and then less abruptly reaching a constant value of 0.50 $cm^3\ K\ mol^{-1}$ at 50 K. This behavior indicates the occurrence of an almost complete HS-to-LS conversion. The $\chi_M T$ value at low temperature is consistent with the occurrence of 15% Fe^{II} centers in the HS state. The warming mode does not match the cooling mode denoting the presence of an unsymmetrical hysteresis, which suggests some cooperativity. The critical temperatures obtained from $\partial\chi MT/\partial T$ are $T_c\downarrow = 218$ K and $T_c\uparrow = 226$ K, indicating the occurrence of a hysteresis 8 K wide (temperature scan rate of 1 K/min).

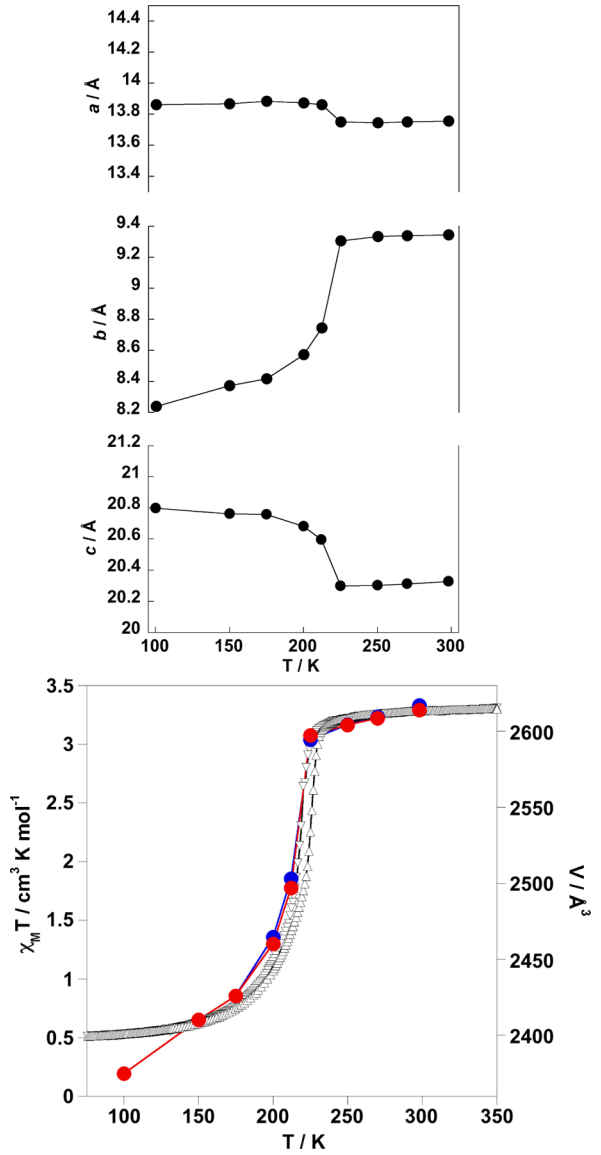

Figure 5. Thermal variation of the crystal parameters a, b, and c (top) and overlay of the thermal variation of the unit cell volume (V) and $\chi_M T$ (bottom) for **2**.

Photogeneration of the metastable HS* state at low temperature, the so-called light-induced excited spin state

DOI: 10.1021/acs.inorgchem.5b01001
Inorg. Chem. 2015, 54, 7424−7432

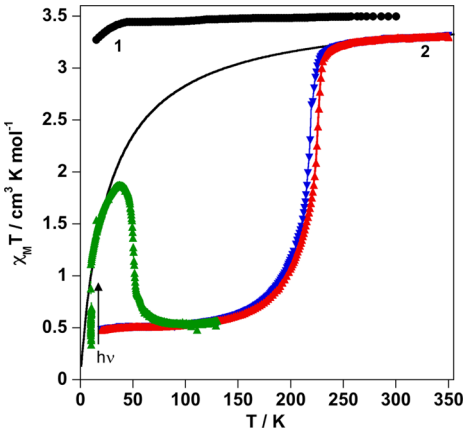

Figure 6. $\chi_M T$ vs T plots for **1** and **2** measured at 1 K min^{-1}. Blue and red triangles represent the cooling and heating modes. Green triangles correspond to the photomagnetic experiment. Solid line corresponds to simulation of antiferromagnetic coupling in a 2D system (see text).

trapping experiment (LIESST),[26] was carried out on a microcrystalline sample (0.70 mg) of **1**. The sample was cooled in the dark down to 10 K. At this temperature $\chi_M T \approx 0.30$ cm^3 K mol^{-1}. Then the sample was irradiated with green light (λ = 532 nm) for 3 h, the time required to attain a saturation value of ca. $\chi_M T \approx 1.10$ cm^3 K mol^{-1}. The light irradiation was then switched off and the temperature increased at a rate of 0.3 K min^{-1}. In the 10−39 K temperature range $\chi_M T$ increases reaching a maximum value of ca. 1.90 cm^3 K mol^{-1} at 39 K. This increase of $\chi_M T$ essentially indicates a thermal population of the different microstates arising from weak Fe^{II}−Fe^{II} antiferromagnetic coupling through the tetrazolate rings, which is expected to occur in the 2D single-bridged [Fe(tetrazolate)]$_\infty$ layers.[27] Indeed, Lines' quadratic-layer antiferromagnet law[28] gives a reasonable good simulation of the experimental data in the temperature intervals 350−230 K and 27−10 K with parameters g = 2 and $2J$ = −2 cm^{-1} (solid line in Figure 1). This fact suggests that the light-induced population of the HS state is virtually complete at 10 K. Antiferromagnetic coupling in the HS* state was first observed in the dinuclear complex {[Fe(bt)(NCS)$_2$]$_2$bpym} (bt = 2,2′-bithiazoline and bpym = bipyrimidine).[29] Similar antiferromagnetic coupling through pyrimidine bridge was described for the HS* state in the 3D coordination polymer {Fe(pyrimidine)[Ag(CN)$_2$][Ag$_2$(CN)$_3$]}.[30] At temperatures greater than 39 K, $\chi_M T$ drops rapidly and reaches a value about 0.50 cm^3 K mol^{-1} at ca. 86 K indicating complete HS* → LS relaxation. The T_{LIESST} temperature[26b] determined from the maximum variation of $\chi_M T$ in the HS → LS relaxation is equal to 52 K.

Mössbauer Spectra. Representative ^{57}Fe Mössbauer spectra of samples of **1** (293 K) and **2** (80 K, 293 K) are shown in Figure 7. Values of the Mössbauer parameters have been obtained by least-squares fitting of the spectra. At 80 K, the characteristic Mössbauer spectrum of **2** consists of two quadrupole-split doublets with isomer shifts δ = 0.467(1) and 1.153(1) mm s^{-1} with corresponding quadrupole splitting ΔE_Q = 0.685(3) and 2.48(2) mm s^{-1}, which are consistent with one LS and one HS site (Figure 7a), respectively. The relative area of the LS doublet (A/A_{tot}) is 85.5(6)% while the corresponding relative area for the HS doublet represents the remaining 14.5(9)% of the total spectrum. At 293 K, the spectrum was fitted to one HS doublet with δ = 0.977(5) and ΔE_Q =

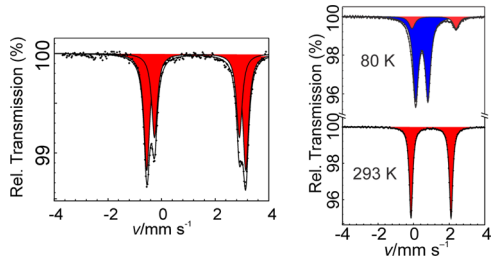

Figure 7. Mössbauer spectra of **1** (left) and **2** (right). Red and blue colors denote the HS and LS states, respectively.

2.250(1) mm s^{-1}. In agreement with the magnetic curve and crystallographic data of **2**, these values clearly show the presence of a residual fraction of Fe^{II} centers in the HS state at 80 K (ca. 15%) and complete conversion to the HS state at 293 K. Consistently, extrapolation of ΔR = 0.174 Å to 100% of SCO gives 0.205 Å, a quite reasonable average Fe−N bond length change. The Mössbauer spectrum of **1** at 293 K was fitted to two doublets characterized by δ_1 = 1.2973(21) mm s^{-1}, ΔE_{Q1} = 3.6887(62) mm s^{-1}, $(A/A_{tot})_1$ = 58.7(24)%, and δ_2 = 1.3206(29) mm s^{-1}, ΔE_{Q2} = 3.1628(84) mm s^{-1}, $(A/A_{tot})_2$ = 41.3(23)%. These δ and ΔE_Q values are similar to those observed for the complexes [Fe(L-N$_4$H$_2$)](BPh$_4$)$_2$·Et$_2$O (δ = 1.24(1) mm s^{-1}, ΔE_{Q2} = 3.05(1) mm s^{-1})[20] and [Fe(LN$_4$)$_2$](BF$_4$)$_2$ (δ = 1.56(6) mm s^{-1}, ΔE_Q = 3.85(2) mm s^{-1}).[21] For the complex [Fe(cyclen-py$_4$](ClO$_4$)$_2$·H$_2$O,[25] which displays a 6 + 2 coordination environment characterized by two long Fe−Npy bond distances of about 3 Å, δ and ΔE_Q are, respectively, 1.007 and 3.20 mm s^{-1}. The complex [Fe(1,8-naphtypyridine)$_4$(ClO$_4$)$_2$] displays the largest ΔE_Q = 4.54 mm s^{-1} observed for an octacoordinate Fe^{II} ion, 4.54 mm s^{-1}.[31]

Calorimetric Properties. The calorimetric measurements were carried out in the 120−300 K temperature range at a temperature scan rate 10 K min^{-1}. A smooth line has been interpolated from the values in the normal regions, below 140 K and above 260 K. The heat capacity due to the transition has been deduced by subtraction of this baseline. The temperature dependence of the resultant excess of heat capacity, ΔC_p, in the cooling and heating modes for **2** is displayed in Figure 8. The enthalpy variation, ΔH, associated with the spin transition determined from the area under the DSC curves and the critical temperatures, T_c, obtained from the maximum of ΔC_p versus T curve are $\Delta H\downarrow$ = 7.6 ± 0.4 kJ mol^{-1} ($T_c\downarrow$ = 215 K) and $\Delta H\uparrow$ = 8.9 ± 0.4 kJ mol^{-1} ($T_c\uparrow$ = 225.4 K) for the cooling and heating modes, respectively. From these values, entropy variations (ΔS

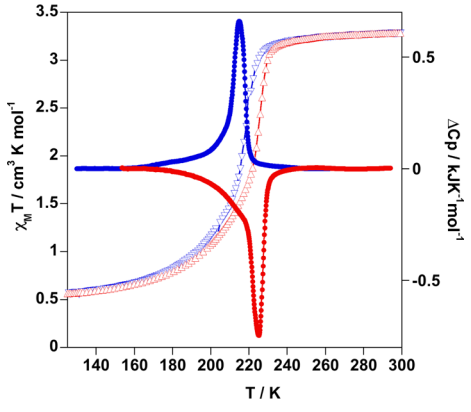

Figure 8. Overlay of ΔC_p and $\chi_M T$ vs T plots for **2**.

DOI: 10.1021/acs.inorgchem.5b01001
Inorg. Chem. 2015, 54, 7424−7432

= $\Delta H/T_c$) of 35.5 ± 3 J K^{-1} mol^{-1} and 39.5 ± 3 J K^{-1} mol^{-1} were found for each mode, respectively. The difference between the cooling and heating temperatures, $\Delta T_c = T_c\uparrow - T_c\downarrow \approx 10$ K, suggests the occurrence of a hysteresis loop slightly larger than that found from magnetic data. This discrepancy is due to the large difference of temperature scan rates used in both experiments for **2**. These values are reasonably consistent with those obtained from the $\chi_M T$ versus T plot. The average values of the thermodymamic parameters are ΔH^{av} = 8.27 kJ mol^{-1}, ΔS^{av} = 37.5 J K^{-1} mol^{-1}, and T_c^{av} = 220.2 K. The ΔS^{av}, and therefore ΔH^{av}, is slightly smaller than expected for moderately cooperative SCO.[32] This fact is explained by ca. 15% Fe^{II} centers remaining in the HS at low temperatures. Indeed, $\Delta H_{100\%}$ = 9.7 kJ mol^{-1} and $\Delta S_{100\%}$ = 44.1 J K^{-1} mol^{-1} when the spin transition is extrapolated to 100% conversion.

CONCLUSION

In summary, we have described the synthesis and characterization of two radically distinct Fe^{II} homoleptic complexes derived from the deprotonable tetradentate ligand [H_2bipy(ttr)$_2$]. Deprotonation with EtN_3 affords compound **1**, constituted of discrete mononuclear anionic {Fe[bipy(ttr)$_2$][Hbipy(ttr)$_2$]}$^-$ complex units, $[Et_3NH]^+$ cations and MeOH molecules. The Fe^{II}, surrounded by 8 N atoms, defines a distorted bisdisphenoid dodecahedron, which is relatively uncommon in the stereochemistry of Fe^{II}. The magnetic properties of **1** are consistent with the S = 2 state of the Fe^{II} ion, and the Mössbauer spectrum is characterized by relatively large ΔE_Q values consistent with those of the other related compounds. Full self-deprotonation of the ligand during slow diffusion process afforded compound **2**. At variance with **1**, only one [bipy(ttr)$_2$]$^{2-}$ anion embraces the Fe^{II} ion occupying the equatorial coordination positions in **2**. Two tetrazolate rings of two adjacent equivalent Fe[bipy(ttr)$_2$] moieties fill the remaining axial positions of a strongly distorted octahedral center, thereby constituting a double-layered two-dimensional coordination polymer. In contrast to **1**, compound **2** undergoes moderately cooperative thermal-induced SCO behavior. At temperatures below 40 K the photoinduced HS state denotes the occurrence of weak antiferromagnetic interactions between the Fe^{II} centers mediated through the tetrazolate rings. As far as we know compound **2** represents the second example, together with [Fe(2,4-bpt)$_2$]·$n$$H_2O$,[18] of a two-dimensional Fe^{II} SCO coordination polymer made up exclusively of an ionogenic ligand.

EXPERIMENTAL SECTION

Materials. Solvents and starting materials were purchased from commercial sources and used without further purification. The ligand H_2bipy(ttr)$_2$ was synthesized according to the reported procedure.[19]

For the synthesis of **1**, a suspension of ligand H_2bipy(ttr)$_2$ (73.1 mg, 0.25 mmol) in methanol (6 mL) was reacted with triethylamine (69.7 mL, 0.5 mmol) to obtain a colorless solution. After addition of a solution of the Fe$(BF_4)_2$·6H_2O (42.3 mg, 0.12 mmol) in methanol (2 mL), the resulting orange-brown solution was left standing at room temperature for several days. The NEt_3H{Fe[Hbipy(ttr)$_2$][H_2bipy(ttr)]}·3MeOH complex obtained as orange crystals was filtered and washed with a little methanol. Yield 51.0 mg (49%). Anal. Calcd (%) for $C_{42}H_{35}Fe_2N_{31}$: C, 48.72; H, 3.95; N, 39.77. Found: C, 48.42; H, 4.01; N, 40.04.

For the synthesis of **2**, there are two methods: (A) Microcrystalline precipitated samples of **2** have been obtained by adding dropwise a filtered solution of Fe$(BF_4)_2$·6H_2O (20.0 mg, 0.06 mmol) in 5 mL of DMF to boiling solution of H_2bipy(ttr)$_2$ (17.3 mg, 0.06 mmol) in 5 mL of DMF. Yield 15.2 mg (72%). (B) Alternatively, single crystals of **2** have been obtained by diffusion methods as follows: an H-shaped vessel with solid Fe$(BF_4)_2$·6H_2O (20.0 mg, 0.06 mmol) in one side and solid ligand [H_2bipy(ttr)$_2$] (17.3 mg, 0.06 mmol) in the other arm was filled with methanol. Well-shaped dark violet crystals suitable for single crystal X-ray analysis were obtained after 3 months. Yield ca. 2.1 mg (10%). Anal. Calcd (%) for $C_{12}H_6FeN_{10}$: C, 41.65; H, 1.75; N, 40.47. Found: C, 41.97; H, 1.61; N, 40.65.

Physical Measurements. Variable temperature magnetic susceptibility data were recorded at a rate of 1 K min^{-1} with a Quantum Design MPMS2 SQUID susceptometer equipped with a 7 T magnet, operating at 1 T and at temperatures 2−400 K. Experimental susceptibilities were corrected from diamagnetism of the constituent atoms by the use of Pascal's constants. TGA measurements were performed on a Mettler Toledo TGA/SDTA 851e, in the 290−800 K temperature range under a nitrogen atmosphere with a rate of 10 K min^{-1}. Differential scanning calorimetry (DSC) measurements were performed on a dry sample of **2** using a Mettler Toledo DSC 821e calorimeter. Low temperatures were obtained with an aluminum block which was attached to the sample holder, refrigerated with a flow of liquid nitrogen, and stabilized at a temperature of 110 K. The sample holder was kept in a drybox under a flow of dry nitrogen gas to avoid water condensation. The measurements were carried out using about 10 mg of crystalline samples sealed in aluminum pans with a mechanical crimp. The temperature scan rate was 10 K/min. Overall accuracies of 0.2 K in the temperature and 2% in the heat capacity are estimated. The uncertainty increases for the determination of the anomalous enthalpy and entropy due to the subtraction of an unknown baseline. ^{57}Fe Mössbauer spectra were recorded in transmission geometry with a ^{57}Co/Rh source kept at room temperature and a conventional spectrometer operating in the constant-acceleration mode. The samples were sealed in a Plexiglas sample holder and mounted in a nitrogen-bath cryostat. The spectrum evaluations were done with the assumption of Lorentzian line shapes using the Recoil 1.05 Mössbauer Analysis Software (Dr. E. Lagarec, http://www.isapps.ca/recoil/). All isomer shifts are given relative to α-Fe at room temperature. Microanalyses were performed using a LECO CHNS-932 analyzer.

Single crystal X-ray data of **1** were collected on an Oxford Diffraction Supernova single crystal diffractometer using Mo Kα radiation (λ = 0.710 73 Å). The experiment for **2** was carried out with a wavelength λ = 0.7999 Å, between 100 K and room temperature, at the 911-3 beamline of the Max II Synchrotron (MAX IV Laboratory, Lund, Sweden) using a MAR225 CCD area detector, making ϕ scans while collecting the data.[33] A data scaling and empirical or multiscan absorption correction was performed. The structures were solved by direct methods using SHELXS-97 and refined by full-matrix least-squares on F^2 using SHELXL-97.[34] Non-hydrogen atoms were refined anisotropically. H1 and H2 hydrogen atoms were located by Fourier difference synthesis, and the remaining H atoms were geometrically placed (riding model) and assigned fixed isotropic displacement parameters.

ASSOCIATED CONTENT

Supporting Information

Crystallographic information files (CIFs). The Supporting Information is available free of charge on the ACS Publications website at DOI: 10.1021/acs.inorgchem.5b01001.

AUTHOR INFORMATION

Corresponding Authors

*E-mail: mcs@univ.kiev.ua, mlseredyuk@gmail.com.
*E-mail: jose.a.real@uv.es.

Author Contributions

The manuscript was written through contributions of all authors.

DOI: 10.1021/acs.inorgchem.5b01001
Inorg. Chem. 2015, 54, 7424−7432

Notes

The authors declare no competing financial interest.

■ ACKNOWLEDGMENTS

The research reported here was supported by the Spanish Ministerio de Economía y Competitividad (MINECO) and FEDER funds (CTQ2013-46275-P) and Generalitat Valenciana (PROMETEO/2012/049). L.P.-L. thanks the Generalitat Valenciana and the Universidad de Valencia for a predoctoral fellowship. M.S. thanks the EU for a Marie Curie fellowship (IIF-253254).

■ REFERENCES

(1) See for example: (a) Goodwin, H. A. *Coord. Chem. Rev.* **1976**, *18*, 293−325. (b) Gütlich, P. *Struct. Bonding (Berlin)* **1981**, *44*, 83−195. (c) König, E.; Ritter, G.; Kulshreshtha, S. K. *Chem. Rev.* **1985**, *85*, 219−234. (d) Hauser, A. *Comments Inorg. Chem.* **1995**, *17*, 17−40. (e) König, E. *Struct. Bonding (Berlin)* **1991**, *76*, 51−157. (f) Gütlich, P.; Hauser, A.; Spiering, H. *Angew. Chem., Int. Ed. Engl.* **1994**, *33*, 2024−2054. (g) Sato, O. *Acc. Chem. Res.* **2003**, *36*, 692−700. (h) Real, J. A.; Gaspar, A. B.; Niel, V.; Muñoz, M. C. *Coord. Chem. Rev.* **2003**, *236*, 121−141. (i) Gütlich, P.; Goodwin, H. A. Eds., *Top. Curr. Chem.* 2004, Vols. *233*−*235*;. (j) Real, J. A.; Gaspar, A. B.; Muñoz, M. C. *Dalton Trans.* **2005**, 2062−2079. (k) Halcrow, M. A. *Coord. Chem. Rev.* **2009**, *253*, 2493−2514. (l) Olguin, J.; Brooker, S. *Coord. Chem. Rev.* **2011**, *255*, 203−240. (m) Bousseksou, A.; Molnár, G.; Salmon, L.; Nicolazzi, W. *Chem. Soc. Rev.* **2011**, *40*, 3313−3335. (m) *Spin-Crossover Materials: Properties and Applications*; Halcrow, M. A., Ed.; Wiley: Chichester, U.K., 2013.

(2) See for example: (a) Kahn, O.; Jay-Martinez, C. *Science* **1998**, *279*, 44−48. (b) Galet, A.; Gaspar, A. B.; Muñoz, M. C.; Bukin, G. V.; Levchenko, G.; Real, J. A. *Adv. Mater.* **2005**, *17*, 2949−2953. (c) Matsuda, M.; Isozaki, H.; Tajima, H. *Thin Solid Films* **2008**, *517*, 1465−1467. (d) Ni, Z.; Shores, M. P. *J. Am. Chem. Soc.* **2009**, *131*, 32−33. (e) Ohba, M.; Yoneda, K.; Agustí, G.; Muñoz, M. C.; Gaspar, A. B.; Real, J. A.; Yamasaki, M.; Ando, H.; Nakao, Y.; Sakaki, S.; Kitagawa, S. *Angew. Chem., Int. Ed.* **2009**, *48*, 4767−4771. (f) Gaspar, A. B.; Seredyuk, M.; Gütlich, P. *Coord. Chem. Rev.* **2009**, *253*, 2399−2413. (g) Garcia, Y.; Robert, F.; Naik, A. D.; Zhou, G.; Tinant, B.; Robeyns, K.; Michotte, S.; Piraux, L. *J. Am. Chem. Soc.* **2011**, *133*, 15850−15853. (h) Titos-Padilla, S.; Herrera, J. M.; Chen, X. W.; Delgado, J. J.; Colacio, E. *Angew. Chem., Int. Ed.* **2011**, *50*, 3290−3293. (i) Linares, J.; Codjovi, E.; Garcia, Y. *Sensors* **2012**, *12*, 4479−4492. (j) Hayami, S. In *Spin-Crossover Materials: Properties and Applications*; Halcrow, M., Ed.; Wiley: Chichester, U.K., 2013; pp 321−345. (k) Shepherd, H. J.; Quintero, C. M.; Molnár, G.; Salmon, L.; Bousseksou, A. In *Spin-Crossover Materials: Properties and Applications*; Halcrow, M., Ed.; Wiley: Chichester, U.K., 2013; pp 347−373.

(3) See for example: (a) Cavallini, M. *Phys. Chem. Chem. Phys.* **2012**, *14*, 118867−11867. (b) Ruiz, E. *Phys. Chem. Chem. Phys.* **2014**, *16*, 14−22. (c) Martinho, P. N.; Rajnak, C.; Ruben, M. In *Spin-Crossover Materials: Properties and Applications*; Halcrow, M., Ed.; Wiley: Chichester, U.K., 2013; pp 375−404. (d) Shepherd, H. J.; Molnár, G.; Nicolazzi, W.; Salmon, L.; Bousseksou, A. *Eur. J. Inorg. Chem.* **2013**, *2013*, 653−661. (e) Rotaru, A.; Dugay, J.; Tan, R. P.; Gural'skiy, I. A.; Salmon, L.; Demont, P.; Carrey, J.; Molnár, G.; Respaud, M.; Bousseksou, A. *Adv. Mater.* **2013**, *25*, 1745−1749. (f) Gural'skiy, I. A.; Quintero, C. M.; Sánchez Costa, J.; Demont, P.; Molnár, G.; Salmon, L.; Shepherd, H. J.; Bousseksou, A. *J. Mater. Chem. C* **2014**, *2*, 2949−2955. (g) Bartual-Murgui, C.; Akou, A.; Thibault, C.; Molnár, G.; Vieu, C.; Salmon, L.; Bousseksou, A. *J. Mater. Chem. C* **2015**, *3*, 1277−1285.

(4) Halcrow, M. A. *Polyhedron* **2007**, *26*, 3523−3576.

(5) Benmansour, S.; Atmani, C.; Setifi, F.; Triki, S.; Marchivie, M.; Gómez-García, C. J. *Coord. Chem. Rev.* **2010**, *254*, 1468−1478.

(6) Muñoz, M. C.; Real, J. A. In *Spin-Crossover Materials: Properties and Applications*; Halcrow, M., Ed.; Wiley: Chichester, U.K., 2013; pp 122−146.

(7) Muñoz, M. C.; Real, J. A. *Coord. Chem. Rev.* **2011**, *255*, 2068−2093.

(8) (a) Hutchinson, B.; Daniels, L.; Henderson, E.; Neill, P.; Long, G. J.; Becker, L. W. *J. Chem. Soc., Chem. Commun.* **1979**, 1003−1004. (b) Grandjean, F.; Long, G. J.; Hutchinson, B. B.; Ohlhausen, L.; Neill, P.; Holcomb, J. D. *Inorg. Chem.* **1989**, *28*, 4406−4414.

(9) (a) Real, J. A.; Muñoz, M. C.; Faus, J.; Solans, X. *Inorg. Chem.* **1997**, *36*, 3008−3013. (b) Moliner, N.; Salmon, L.; Capes, L.; Muñoz, M. C.; Létard, J. F.; Bousseksou, A.; Tuchagues, J. P.; McGarvey, J. J.; Dennis, A. C.; Castro, M.; Burriel, R.; Real, J. A. *J. Phys. Chem. B* **2002**, *106*, 4276−4283. (c) Thompson, A. L.; Goeta, A. E.; Real, J. A.; Galet, A.; Muñoz, M. C. *Chem. Commun.* **2004**, 1390−1391.

(10) (a) Naggert, H.; Bannwarth, A.; Chemnitz, S.; von Hofe, T.; Quandt, E.; Tuczek, F. *Dalton Trans.* **2011**, *40*, 6364−6366. (b) Palamarciuc, T.; Oberg, J. C.; El Hallak, F.; Hirjibehedin, C. F.; Serri, M.; Heutz, S.; Létard, J. F.; Rosa, P. *J. Mater. Chem.* **2012**, *22*, 9690−9695.

(11) (a) Meded, V.; Bagrets, A.; Fink, K.; Chandrasekar, R.; Ruben, M.; Evers, F.; Bernand-Mantel, A.; Seldenthuis, J. S.; Beukman, A.; van der Zant, H. S. J. *Phys. Rev. B: Condens. Matter Mater. Phys.* **2011**, *83*, 245415. (b) Prins, F.; Monrabal-Capilla, M.; Osorio, E. A.; Coronado, E.; van der Zant, H. S. J. *Adv. Mater.* **2011**, *23*, 1545−1549. (c) Gopakumar, T. G.; Matino, F.; Naggert, H.; Bannwarth, A.; Tuczek, F.; Berndt, R. *Angew. Chem., Int. Ed.* **2012**, *51*, 6262−6266. (d) Miyamachi, T.; Gruber, M.; Davesne, V.; Bowen, M.; Boukari, S.; Joly, L.; Scheurer, F.; Rogez, G.; Yamada, T. K.; Ohresser, P.; Beaurepaire, E.; Wulfhekel, W. *Nat. Commun.* **2012**, *3*, 938.

(12) Schäfer, B.; Rajnák, C.; Šalitroš, I.; Fuhr, O.; Klar, D.; Schmitz-Antoniak, C.; Weschke, E.; Wende, H.; Ruben, M. *Chem. Commun.* **2013**, *49*, 10986−10988.

(13) Seredyuk, M.; Znovjyak, K. O.; Kusz, J.; Nowak, M.; Muñoz, M. C.; Real, J. A. *Dalton Trans.* **2014**, *43*, 16387−16394.

(14) Boinnard, D.; Bousseksou, A.; Dworkin, A.; Savariault, J. M.; Varret, F.; Tuchagues, J. P. *Inorg. Chem.* **1994**, *33*, 271−281.

(15) Weber, B. *Coord. Chem. Rev.* **2009**, *253*, 2432−2449.

(16) (a) Zhang, L.; Xu, G. C.; Xu, H. B.; Mereacre, V.; Wang, Z. M.; Powell, A. K.; Gao, S. *Dalton Trans.* **2010**, *39*, 4856−4868. (b) Zhang, L.; Xu, G. C.; Xu, H. B.; Zhang, T.; Wang, Z. M.; Yuan, M.; Gao, S. *Chem. Commun.* **2010**, *46*, 2554−2556. (c) Zhang, L.; Xu, L.; Wang, G. C.; Gao, Z. M. *Eur. J. Inorg. Chem.* **2013**, *2013*, 1043−1048.

(17) Patrick, B. O.; Reiff, W. M.; Sanchez, V.; Storr, A.; Thompson, R. C. *Inorg. Chem.* **2004**, *43*, 2330−2339.

(18) (a) Bao, X.; Liu, J. L.; Leng, J. D.; Lin, Z.; Tong, M. L.; Nihei, M.; Oshio, H. *Chem. - Eur. J.* **2010**, *16*, 7973−7978. (b) Bao, X.; Guo, P. H.; Liu, J. L.; Leng, J. D.; Tong, M. L. *Chem. - Eur. J.* **2011**, *17*, 2335−2339.

(19) Andreiadis, E. S.; Demadrille, R.; Imbert, D.; Pecaut, J.; Mazzanti, M. *Chem. - Eur. J.* **2009**, *15*, 9458−9476.

(20) Koch, W.; Barbieri, A.; Grodzicki, M.; Schunemann, V.; Trautwein, A. X.; Krüger, H. J. *Angew. Chem., Int. Ed. Engl.* **1996**, *35*, 422−424.

(21) Patra, A. K.; Dube, K. S.; Papaefthymiou, G. C.; Conradie, J.; Ghosh, A.; Harrop, T. C. *Inorg. Chem.* **2010**, *49*, 2032−2034.

(22) Clearfield, A.; Singh, P.; Bernal, I. *J. Chem. Soc. D* **1970**, 389−390.

(23) Di Vaira, M.; Mani, F.; Stoppioni, P. *J. Chem. Soc., Dalton Trans.* **1992**, 1127−1130.

(24) Diebold, A.; Hagen, K. S. *Inorg. Chem.* **1998**, *37*, 215−223.

(25) Bu, X. H.; Lu, S. L.; Zhang, R. H.; Liu, H.; Zhu, H. P.; Liu, Q. T. *Polyhedron* **2000**, *19*, 431−435.

(26) (a) Hauser, A. *Top. Curr. Chem.* **2004**, *234*, 155−198. (b) Létard, J. F. *J. Mater. Chem.* **2006**, *16*, 2550−2559. (c) Létard, J. F.; Guionneau, P.; Nguyen, O.; Costa, J. S.; Marcen, S.; Chastanet, G.; Marchivie, M.; Goux-Capes, L. *Chem. - Eur. J.* **2005**, *11*, 4582−4589.

(27) Gao, E. Q.; Liu, N.; Cheng, A. L.; Gao, S. *Chem. Commun.* **2007**, 2470−2472.

(28) Lines, M. E. *J. Phys. Chem. Solids* **1970**, *31*, 101−116.

(29) (a) Létard, J. F.; Real, J. A.; Moliner, N.; Gaspar, A. B.; Capes, L.; Cador, O.; Kahn, O. *J. Am. Chem. Soc.* **1999**, *121*, 10630−10631.

DOI: 10.1021/acs.inorgchem.5b01001
Inorg. Chem. 2015, 54, 7424−7432

(b) Chastanet, G.; Gaspar, A. B.; Real, J. A.; Létard, J. F. *Chem. Commun.* **2001**, 819−820.
(30) Niel, V.; Thompson, A. L.; Goeta, A. E.; Enachescu, C.; Hauser, A.; Galet, A.; Muñoz, M. C.; Real, J. A. *Chem. - Eur. J.* **2005**, *11*, 2047−2060.
(31) Konig, E.; Ritter, G.; Lindner, E.; Lorenz, I. P. *Chem. Phys. Lett.* **1972**, *13*, 70−72.
(32) (a) Sorai, M.; Seki, S. *J. Phys. Chem. Solids* **1974**, *35*, 555−570. (b) Sorai, M.; Nakano, M.; Miyazaki, Y. *Chem. Rev.* **2006**, *106*, 976−1031. (c) Sorai, M. *Top. Curr. Chem.* **2004**, *235*, 153−170.
(33) Ursby, T.; Unge, J.; Appio, R.; Logan, D. T.; Fredslund, F.; Svensson, C.; Larsson, K.; Labrador, A.; Thunnissen, M. M. G. M. *J. Synchrotron Radiat.* **2013**, *20*, 648−653.
(34) Sheldrick, G. M. *Acta Crystallogr., Sect. A: Found. Crystallogr.* **2008**, *64*, 112−122.

DOI: 10.1021/acs.inorgchem.5b01001
Inorg. Chem. 2015, 54, 7424−7432